

# Seismicity around the trench axis and outer-rise region of the southern Japan Trench, south of the main rupture area of the 2011 Tohoku-oki earthquake

Koichiro Obana<sup>1b</sup>, Gou Fujie<sup>1b</sup>, Yojiro Yamamoto<sup>1b</sup>, Yuka Kaiho, Yasuyuki Nakamura<sup>1b</sup>, Seiichi Miura<sup>1b</sup> and Shuichi Kodaira<sup>1b</sup>

*Research Institute for Marine Geodynamics (IMG), Japan Agency for Marine-Earth Science and Technology (JAMSTEC), Yokohama 236-0001, Japan.  
E-mail: obanak@jamstec.go.jp*

Accepted 2021 March 5. Received 2021 February 25; in original form 2020 October 2

## SUMMARY

The 2011  $M_w$  9.0 Tohoku-oki earthquake ruptured the subduction megathrust fault in the central Japan Trench. We investigated the aftershock activity in the southern Japan Trench to the south of the main rupture area using ocean bottom seismographs deployed both landward and seaward of the trench. In the trench-outer rise region seaward of the trench axis, we identified several  $\sim 100$ -km-long linear earthquake trends both parallel and oblique to the southern Japan Trench. The earthquake trend oblique to the southern Japan Trench is a southward extension of the trench-parallel linear earthquake trend in the central to northern Japan Trench. The trench-parallel normal-faults in the trench-outer rise region could extend linearly, despite the change of the trench strike from N–S to NNE–SSW to the south of the main rupture area. Normal-faults oblique to the trench should be considered as substantial parts of large intraplate normal-faulting earthquakes. In addition, intraplate seismicity coinciding with the lower velocity oceanic mantle suggest that the structure heterogeneity would be indicative of normal-faults extending into the mantle. In the trench landward area, earthquake activity showed along-trench variations. Earthquakes along the shallow megathrust interface near the trench were observed south of  $37^\circ\text{N}$ . These shallow near-trench regular earthquakes, which are located close to the episodic tremors and temporally correlated with the tremor activities, suggest that the afterslip on the plate interface likely extended to the shallow plate interface close to the trench axis. Smaller spatial scale structure heterogeneity, such as the thickness variation in the channel-like low-velocity sedimentary unit, likely relate to the proximity of the regular earthquakes and slow slip which results in the formation of diverse slip behaviours in the shallow subduction zone of the southern Japan Trench.

**Key words:** Japan; Pacific Ocean; Seismicity and tectonics; Dynamics: seismotectonics; Subduction zone processes.

## 1 INTRODUCTION

The 2011  $M_w$  9.0 Tohoku-oki earthquake is a megathrust earthquake that ruptured the subduction zone along the Japan Trench, where the Pacific Plate subducts beneath northeast Japan with a convergence rate of approximately  $9\text{ cm yr}^{-1}$  (Argus *et al.* 2011). This earthquake is characterized by large coseismic slip along the plate boundary fault reaching the trench axis (e.g. Fujiwara *et al.* 2011). The analyses of seismic and geodetic observations show that coseismic slip  $\geq 50\text{ m}$  occurred on the shallow (depth  $\leq 20\text{ km}$ ) subduction thrust fault in the central Japan Trench around  $38^\circ\text{N}$ , and the main rupture area with a large coseismic slip of more than

20 m extended between  $37^\circ\text{N}$  and  $39^\circ\text{N}$  along the trench (e.g. Yagi & Fukahata 2011; Iinuma *et al.* 2012, Fig. 1).

Following the 2011 Tohoku-oki earthquakes, aftershocks and post-seismic deformations were observed along the Japan Trench. In the main rupture area of the central Japan Trench, there were few interplate thrust-faulting aftershocks (Asano *et al.* 2011; Nakamura *et al.* 2016). Seafloor geodetic observations using GPS-acoustic techniques showed westward (landward) movement (Tomita *et al.* 2017; Honsho *et al.* 2019, Fig. 1). Understanding the geometry of the plate interface is important for evaluating the contribution of the afterslip on the deeper part of the megathrust zone (Barbot 2020), but the westward movement is generally explained by

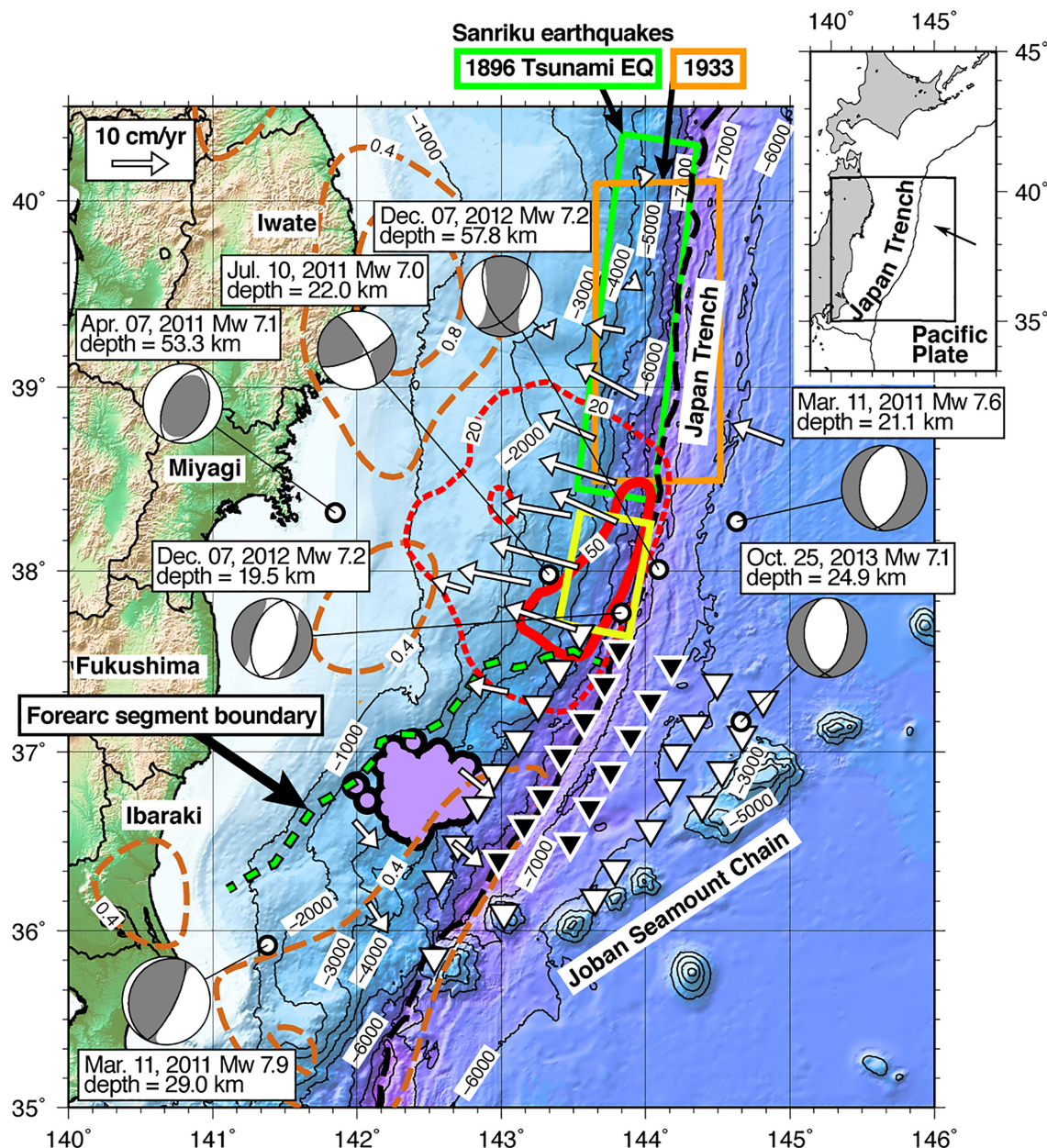


**Figure 1.** Map showing the survey area along the Japan Trench. Open and solid inverted triangles indicate locations of conventional type and ultra-deep-type OBSs, respectively. Only 34 recovered OBSs are indicated. Dotted and solid red lines are the 20- and 50-m contours of coseismic slip distribution of the 2011 Tohoku-oki earthquake (Iinuma *et al.* 2012). Dashed brown contours indicate afterslip distribution of the 2011 Tohoku-oki earthquake from April to December 2011 at 0.4-m intervals (Iinuma *et al.* 2016). Focal mechanisms of M7-class earthquakes after the 2011 Tohoku-oki earthquake until December 2019 taken from the global CMT solutions (Dziewonski *et al.* 1981; Ekström *et al.* 2012) are indicated. Arrows are horizontal displacement rates relative to the North American Plate (Honsho *et al.* 2019). Yellow rectangle is the area of the aseismic wedge inferred from the OBS observations in central Japan Trench (Obana *et al.* 2013). The green dashed line is the structure boundary in the overriding plate by Bassett *et al.* (2016). Purple area indicates the tremor activities by Ohta *et al.* (2019). The green and orange rectangle is the source area of the 1896 Meiji-Sanriku Tsunami (Tanioka & Satake 1996) and 1933 Showa-Sanriku earthquakes (Kanamori 1971), respectively. The dashed black line indicates the Japan Trench axis. The inset is a regional map of the Japan Trench with a convergence vector of Pacific Plate relative to northeast Japan (Argus *et al.* 2011).

post-seismic viscoelastic relaxation following the 2011 earthquake (Sun *et al.* 2014; Agata *et al.* 2019). In addition, several large M7-class intraplate normal-faulting earthquakes, including the  $M_w$  7.6 earthquake 40 min after the 2011 Tohoku-oki earthquake, occurred in the trench-outer rise region of the central Japan Trench (Fig. 1).

In contrast, post-seismic deformation and aftershocks in the southern Japan Trench (south of 37°N) are marked by interplate

aftershocks with thrust-faulting focal mechanisms (Asano *et al.* 2011; Nakamura *et al.* 2016). These interplate aftershocks are likely related to stress concentrations due to the large coseismic slip during the 2011 Tohoku-oki earthquake and the post-seismic slip in the surrounding region. In addition, eastward (seaward) movement in the southern Japan Trench has been observed by post-seismic seafloor geodetic measurements, which is the opposite to the movement observed in the central Japan Trench, indicating an afterslip on the

shallow plate interface in the southern Japan Trench (Sun & Wang 2015; Iinuma *et al.* 2016, Fig. 1). East of the trench axis, normal-faulting aftershocks occurred along the Japan Trench between 36°N and 40°N based on onshore seismic station observations (Asano *et al.* 2011; Nakamura *et al.* 2016). The normal-faulting aftershocks seaward of the trench have a strong relation to the coseismic slip in the shallow part of the megathrust interface near the trench (Sato *et al.* 2012; Sladen & Trevisan 2018).

The earthquake distribution and focal mechanisms after the 2011 Tohoku-oki earthquake have been investigated from seismicity observations using ocean bottom seismographs (OBSs) deployed on both the landward and seaward slopes of the central Japan Trench (Obana *et al.* 2012, 2013, 2014, 2019). The near-trench seismicity landward of the central Japan Trench is characterized by the aseismic wedge, which is a 40–50-km-wide region at the toe of the overriding plate, coinciding with the large (>50 m) coseismic slip area of the 2011 Tohoku-oki earthquake (Obana *et al.* 2013, Fig. 1). In the aseismic wedge, few earthquakes have been observed within the overriding plate and along the plate interface. The aseismic wedge coinciding with the source area of the 1896 Meiji-Sanriku Tsunami earthquake, which ruptured the shallow part of the subduction plate interface near the trench (Tanioka & Satake 1996), has also been shown by the OBS observations in the northern Japan Trench (Obana *et al.* 2018). Apart from the aseismic wedge, active seismicity within the incoming/subducting Pacific Plate has been observed in the trench-outer rise region in the central Japan Trench (Obana *et al.* 2012, 2013, 2014, 2019). These intraplate earthquakes showed a predominance of normal-faulting focal mechanisms down to a depth of approximately 40–50 km. Most of the intraplate earthquakes seaward of the trench occurred along roughly trench-parallel linear trends coinciding with horst and graben structures (Obana *et al.* 2012, 2019), which are the topographic expressions of normal-faults developed by the bending of the incoming/subducting Pacific Plate (e.g. Nakanishi 2011). However, detailed earthquake activities post Tohoku-oki earthquake in the trench-outer rise region of the southern Japan Trench have not been investigated by near-field observations using OBSs. Previous OBS observations in the southern Japan Trench were mainly conducted in the west of the trench, at water depths shallower than 6000 m (Shinohara *et al.* 2005, 2012; Ohta *et al.* 2019). Mizuno *et al.* (2009) had conducted OBS observations east of the trench, but this was prior to the 2011 Tohoku-oki earthquake and used a limited number of the OBSs.

The tectonic environment in the southern Japan Trench is different from that in the central Japan Trench. The Joban seamount chain is in the trench-outer rise region of the southern trench (Fig. 1), and previous active seismic studies have imaged subducted seamounts beneath the trench landward slope (Mochizuki *et al.* 2008; Nishizawa *et al.* 2009). Furthermore, a thick channel-like low-velocity sedimentary unit, likely related to the subducted seamounts, has been imaged by multichannel seismic surveys (Tsuru *et al.* 2002). Mechanical and hydrological effects of seamount subduction are supposed to generate spatial variations in tectonic loading, sediment consolidation and stress state, and affect the distribution of regular earthquakes and aseismic or slow slip in the subduction zone (Sun *et al.* 2020). In addition to the seamount subduction, the strike of the trench axis, which is oriented NNE–SSW in the southern Japan Trench, is different from the N–S oriented trench strike in the central and northern Japan Trench (Fig. 1). This change in the trench strike might affect the intraplate earthquake activities in the trench-outer rise region, which align roughly parallel to the trench axis (Obana *et al.* 2012, 2018). In the trench landward slope,

Bassett *et al.* (2016) identified a southwest–northeast-striking upper plate structure boundary (forearc segment boundary, Fig. 1) and used gravity modeling to reveal that density increases towards the north. Based on the correlation of the forearc segment boundary with slip behaviours of the plate interface, such as the large coseismic slip of the 2011 Tohoku-oki earthquake, distribution of historical large ( $M > 7$ ) earthquakes, and inter-/post-seismic deformations, it is suggested that along-trench variations in seismogenic behaviour is affected by the upper plate structure.

Herein, we report the seismicity near the trench axis to the outer-rise region of the southern Japan Trench, south of the main rupture area of the 2011 Tohoku-oki earthquake, based on the OBS observations. The OBSs were deployed in the trench-outer rise region including the shallow subduction zone near the trench. Although near-field seafloor geodetic data is important to resolve slips in the shallow subduction zones near trenches (Sathiakumar *et al.* 2017), the seafloor geodetic network installed along the Japan Trench is not sufficient to resolve the post-seismic slip after the 2011 Tohoku-oki earthquake in that region (Iinuma *et al.* 2016). Detailed seismic activity based on the near-field observations, such as episodic tremors reported by Ohta *et al.* (2019, Fig. 1), has been used to understand the slip behaviour along the shallow megathrust interface. In the trench-outer rise region, the historic record of large megathrust earthquakes followed by a large intraplate normal-faulting earthquake, such as the 1896 Meiji-Sanriku tsunami and 1933 Showa-Sanriku earthquakes in northern Japan Trench (Fig. 1) and the 2006–2007 Kuril earthquake sequence, raise concerns of a large intraplate normal-faulting earthquake following the 2011 Tohoku-oki earthquake and potential tsunami hazard (Lay *et al.* 2011). The precise earthquake distributions and their focal mechanisms, which can be investigated through earthquake observations using the OBSs, provide information about earthquake activity in the trench-outer rise region and shallow subduction zone near the trench.

## 2 OBSERVATIONS

We conducted earthquake observations using OBSs in the central to southern Japan Trench, off Ibaraki and Fukushima prefectures between 36°N and 38°N by using R/V *Kairei* of Japan Agency for Marine-Earth Science and Technology (JAMSTEC, Fig. 1). We deployed 21 conventional type OBSs with maximum operational depths of 6000 m, and 14 ultra-deep-type OBSs with maximum operational depths of 9000 m (Maeda *et al.* 2013) in March 2017. The OBSs were deployed north of the Joban seamount chain. We recovered 34 OBSs after 4 months (July 2017); one ultra-deep-type OBS was unable to be recovered.

All OBSs were equipped with a three-component 4.5 Hz short-period seismometer. In addition, the conventional OBSs were equipped with a hydrophone. The OBSs recorded signals continuously at a sampling frequency of 100 Hz with a 24-bit analog-to-digital converter. The internal clock of the OBSs were calibrated by linear interpolation of the time differences to the GPS-based reference clock, which was measured just before deployment and shortly after the recovery of each OBS.

## 3 ANALYSIS

Earthquakes were detected from continuous OBS records based on short- and long-term amplitude ratios. We picked phase arrival times manually on the graphical display by using the *WIN* system (Urabe & Tsukada 1992). Where possible, first-motion polarities

and maximum amplitudes were also picked from vertical component seismograms.

First, we determined initial hypocentre locations of approximately 2800 earthquakes using the program *hypomh* (Hirata & Matsu'ura 1987), assuming two 1-D  $P$ -wave velocity ( $V_p$ ) models, one for the OBSs landward of the trench axis and the other for the OBSs seaward of the trench axis, with a fixed  $V_p/V_s$  of 1.78 (Fig. 2). Both models were based on previous studies in the Japan Trench area (Ito *et al.* 2005; Hino *et al.* 2009).

Arrival time delays due to low-velocity sedimentary layers, which were not included in the assumed 1-D  $V_p$  models, were corrected using station values, which were calculated from arrival time differences between direct  $P$ -wave arrival and  $P$ -to- $S$  converted phase at the base of the sedimentary layer, with the assumption of  $V_p$  and  $V_p/V_s$  in the sediments. We used a fixed  $V_p$  of 2.0 km s<sup>-1</sup> in the sediments for all OBSs, and two different  $V_p/V_s$  values in the sediments, 4.4 and 8.0 for the OBSs landward and seaward of the trench axis, respectively. These values were based on previous studies in the Japan Trench area (Obana *et al.* 2012; Nakamura *et al.* 2014). The estimated station corrections were 0.019–0.186 s and 0.317–2.350 s for  $P$ - and  $S$ -wave arrivals, respectively.

After the initial hypocentre estimation based on the 1-D velocity models, we relocated the hypocentres with a 3-D seismic velocity model using double-difference tomography (Zhang & Thurber 2003). This method can estimate both the hypocentre locations and seismic velocity structure from absolute and differential arrival times. We selected 1447 events for the double-difference analysis based on the following two criteria: (1) both  $P$ - and  $S$ -wave arrivals were picked from at least five stations and (2) hypocentres estimated in the initial analysis were near the OBS network, as indicated by the dotted rectangle in Fig. 2(a). The total absolute arrival times for  $P$  and  $S$  waves were 23 591 and 34 058, respectively; the differential arrival times for  $P$  and  $S$  waves were 66 198 and 104 094, respectively.

The double-difference analysis was performed in the 3-D model space with the  $X$ - and  $Y$ -axes roughly normal and parallel to the trench axis, respectively (Fig. S1a). Grid node separations were 12.5 km horizontally and 2–25 km vertically. The initial velocity model used in the double-difference analysis was based on a previous seismic survey along the A6 profile across the study area (Fujie *et al.* 2019, Fig. S1b). The  $V_p$  model along the A6 profile was projected onto the  $X$ -axis and was expanded along the  $Y$ -axis to construct a 3-D velocity model (Fig. S1c). The minimum  $V_p$  at the shallow part was set to be 3.5 km s<sup>-1</sup> in the initial model. Although the  $V_p$  structure along the A6 profile is modeled down to a depth of 30 km, we simply extended the model to depths greater than 30 km by using the velocity at a depth of 30 km. A uniform  $V_p/V_s$  of 1.78 was used in the initial model. Arrival time delays due to the sedimentary layer were corrected using the same station corrections as those used in the initial hypocentre estimations. For both initial and double-difference analyses, the OBSs were located on the seafloor based on the position calibrated during the recovery cruise.

Magnitudes and focal mechanisms were estimated based on the hypocentre locations obtained from the double-difference analysis. The magnitudes of the events were calculated from the maximum amplitude of vertical component seismograms by using an equation for regional earthquakes (Watanabe 1971). We also estimated focal mechanisms from the first-motion polarities of the vertical seismograms using the *HASH* program (Hardebeck & Shearer 2002).

The spatial resolution of the double-difference analysis was examined using a checkerboard resolution test (Figs S2d–f). We applied a  $\pm 5$  per cent velocity perturbation within alternating cells.

The checkerboard interval shown in Figs S2(d)–(f) was 25 km horizontal, and 6–20 km vertical. The synthetic arrival time data used in the checkerboard resolution test included random errors with standard deviations of 0.15 and 0.30 s for  $P$ - and  $S$ -wave arrivals, respectively. These values were based on the root mean square residuals of the double-difference analysis using the OBS observation data. We also examined hypocentre location errors by using 100 bootstrap samples made from absolute arrival time data.

## 4 RESULTS

We obtained relocated hypocentre data for 1437 earthquakes (Fig. 3) with the  $P$ - and  $S$ -wave velocity models from the double-difference analysis (Figs S2a–c). In the following discussion, we use 1239 relocated hypocentres with location errors less than 6 km, which were estimated from the bootstrap samples (Fig. S3). Most of the 913 events had location errors of less than 3 km. The magnitudes of these events ranged from 0.7 to 5.0, and the  $b$ -value was  $0.78 \pm 0.06$ , which was estimated from 705 events with  $M \geq 2.0$  (Aki 1965; Utsu 1965, Fig. 3c). Checkerboard resolution tests show that the velocity models could be resolved within the OBS network down to a depth of approximately 30 and 40 km for seaward and landward of the trench axis, respectively (Figs S2d–f). Longer station separations in the southern part of the OBS network (south of 36.5°N) caused lower resolution compared to the north Fig. S2(d). The velocities outside of the OBS network, such as the area to the south of the Joban seamount chain, were not resolved. The obtained seismic velocity model shows spatial heterogeneities in the uppermost oceanic mantle of the incoming Pacific Plate seaward of the Japan Trench (Figs S2a–c).

Most of the earthquakes were located at depths shallower than 20 km (Fig. 3b), where the seismic activity was widely distributed in the trench-outer rise region. However, earthquake activity in the trench-outer rise region at depths deeper than 25 km, which extended down to approximately 40 km, occurred in a limited area (mainly located in the dotted circle in Fig. 3a, corresponding to the events between 40 and 100 km in horizontal distance on Fig. 3b). Several earthquakes landward of the trench axis were located shallower than the subducting oceanic crust and occurred south of 37°N (Fig. 3a). Some events were located at depths greater than 40 km beneath the trench landward slope. These events correspond to the continuing seismic activity of the lower plane of the double seismic zone in the subducting slab observed in previous OBS observations in the trench landward slope (Shinohara *et al.* 2005).

We obtained the focal mechanisms of 37 events with quality categories A and B [as defined by the *HASH* program by Hardebeck & Shearer (2002)], which correspond to fault plane uncertainties less than 35° (Fig. 4). The data showed a predominance of normal-faulting earthquakes, as shown in the triangle diagram of Frohlich (1992, inset of Fig. 4a), at least north of 36.5°N, where the focal mechanisms were obtained. The data were acquired for depths shallower than 25 km except for one normal-faulting event at 41.7 km depth.

## 5 DISCUSSION

### 5.1 Earthquakes seaward of the trench axis

Similar to the events in the central and northern Japan Trench (Obana *et al.* 2012, 2018, 2019), most earthquakes in the trench-outer rise region of the southern Japan Trench were located at

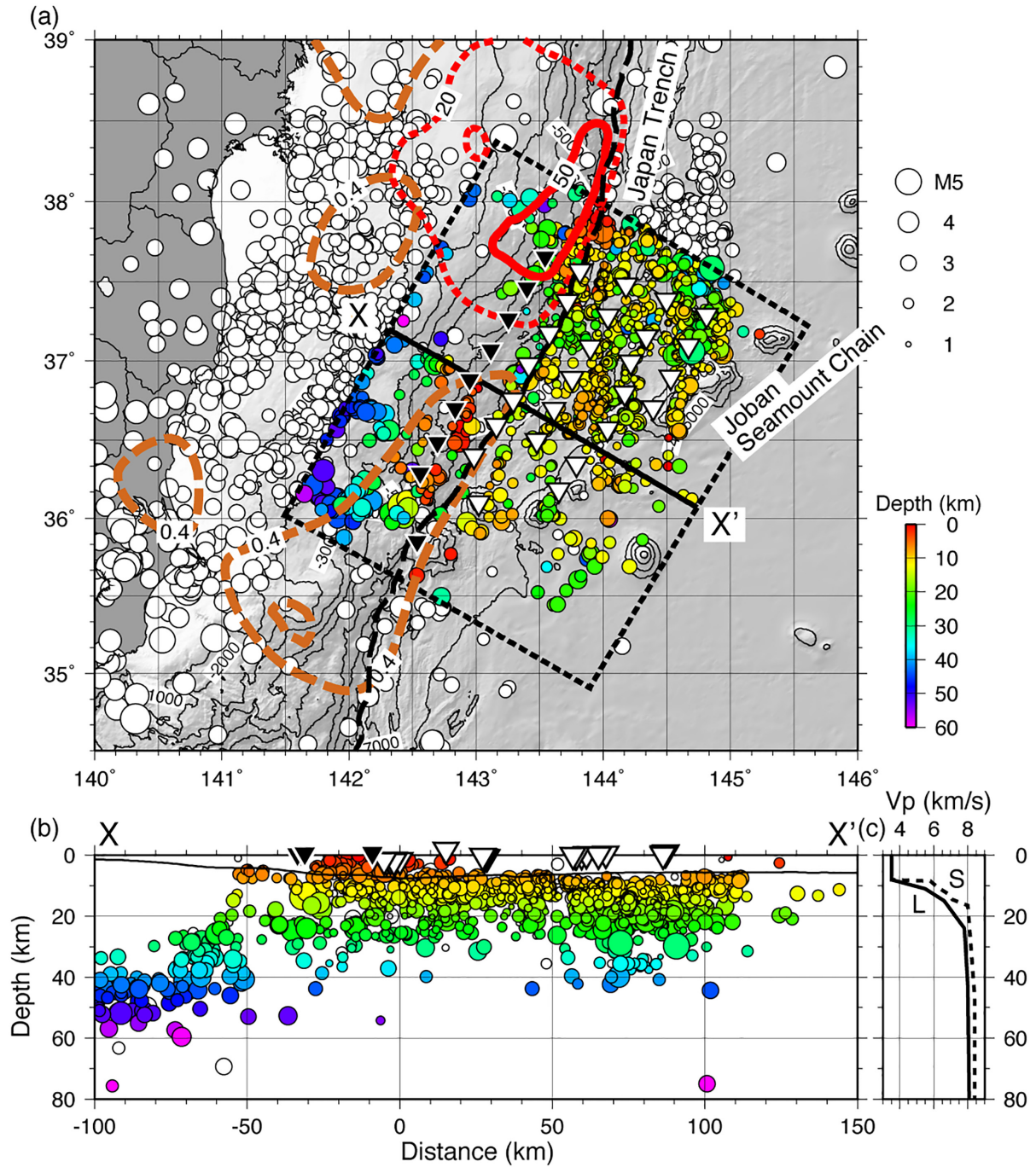


**Figure 2.** Hypocentre distribution estimated by the initial analysis using 1-D velocity models. (a) Map showing hypocentre locations. Circles colour-coded by hypocentre depth are the events used in the double-difference analysis. Dashed black line indicates the trench axis. Open and solid inverted triangles represent OBS locations seaward and landward of the trench axis, respectively. Dotted and solid red lines are the 20- and 50-m contours of coseismic slip distribution of the 2011 Tohoku-oki earthquake (Iinuma *et al.* 2012). Dashed brown contours indicate the afterslip distribution of the 2011 Tohoku-oki earthquake at 0.4-m intervals (Iinuma *et al.* 2016). (b) Cross-section along X–X' profile in the panel (a). Only the events within the dotted rectangle in the panel (a) are indicated. The open and solid inverted triangles indicate OBS locations projected onto the profile X–X'. (c) 1-D *P*-wave velocity models used for the OBSs seaward (S) and landward (L) of the trench axis.

depths shallower than 20 km (Fig. 3). These depths correspond to the oceanic crust and uppermost part of the oceanic mantle of the incoming Pacific Plate. The predominance of the normal-faulting focal mechanisms indicates an extensional stress regime within the oceanic plate, as noted in previous observations. However, the depth extent of the extensional stress regime is not clear because only one

focal mechanism below 30 km was obtained, that is at a depth of 41.7 km (Fig. 4). The hypocentres determined by our OBS observations confirmed that seismicity in the trench-outer rise region extends south to 36°N (Fig. 3), which is consistent with previous studies based on onshore seismic stations after the 2011 Tohoku-oki earthquake (Asano *et al.* 2011; Nakamura *et al.* 2016). Although

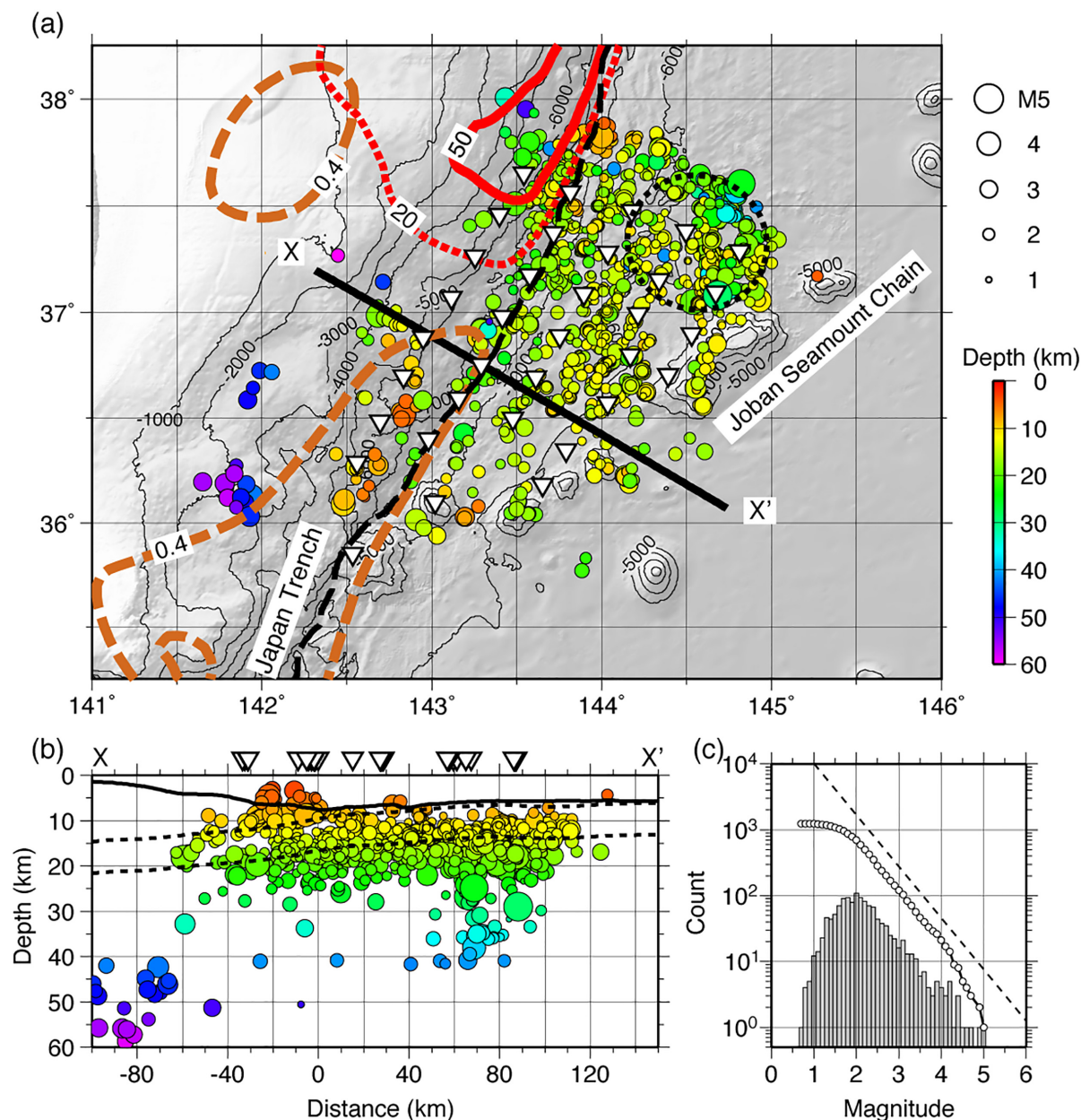


**Figure 3.** Hypocentre distribution and magnitude–frequency diagram obtained from the double-difference analysis. (a) Map showing hypocentre locations. The hypocentres are colour-coded by depth. Inverted triangles are the OBS locations. The dotted circle is the area of the earthquake activities seaward of the trench at depths deeper than 25 km, corresponding to the events between 40 and 100 km in horizontal distance on panel (b). Dotted and solid red lines, and dashed brown and black lines are the same as those in Fig. 2. (b) Hypocentre distribution is projected onto the cross-section along X–X' profile on panel (a), which is located on axis X in Fig. S1(a). Dotted lines roughly correspond to the top of the oceanic crust and oceanic Moho, same with Fig. S2b. (c) Magnitude–frequency diagram. Bars indicate the number of the earthquakes per magnitude range. Open circles are the cumulative number of the earthquakes. Dotted line indicates the slope corresponding to a *b*-value of 0.78.

the hypocentres obtained in this study were located mainly in the area north of the Joban seamount chain (Fig. 3), earthquakes also occurred south of the Joban seamount chain as shown in the initial hypocentre distribution (Fig. 2). The earthquakes south of the Joban seamount chain have larger errors in hypocentre locations because the OBSs were only deployed north of the Joban seamount chain, thus those events were removed from the results of this study shown in Fig. 3 and later.

The earthquakes at depths shallower than 14 km, which correspond to the oceanic crust, show three ~100-km-long linear trends

(A–C in Fig. 5). The general trend of the Japan Trench axis changes by approximately 20° from N–S in the north, to NNE–SSW in the south around 37.5–38.0°N (Fig. 1). The easternmost earthquake trend (trend A), extending in the N–S direction at approximately 144.6°E, is parallel to the N–S trending trench axis to the north. The focal mechanism of the October 2013  $M_w$  7.1 earthquake, from the Global Centroid–Moment–Tensor (CMT) catalogue (Dziewon-ski *et al.* 1981; Ekström *et al.* 2012), and the predominance of the roughly E–W oriented *T*-axes which were obtained from the OBS observations, collocated with the 2013  $M_w$  7.1 earthquake,

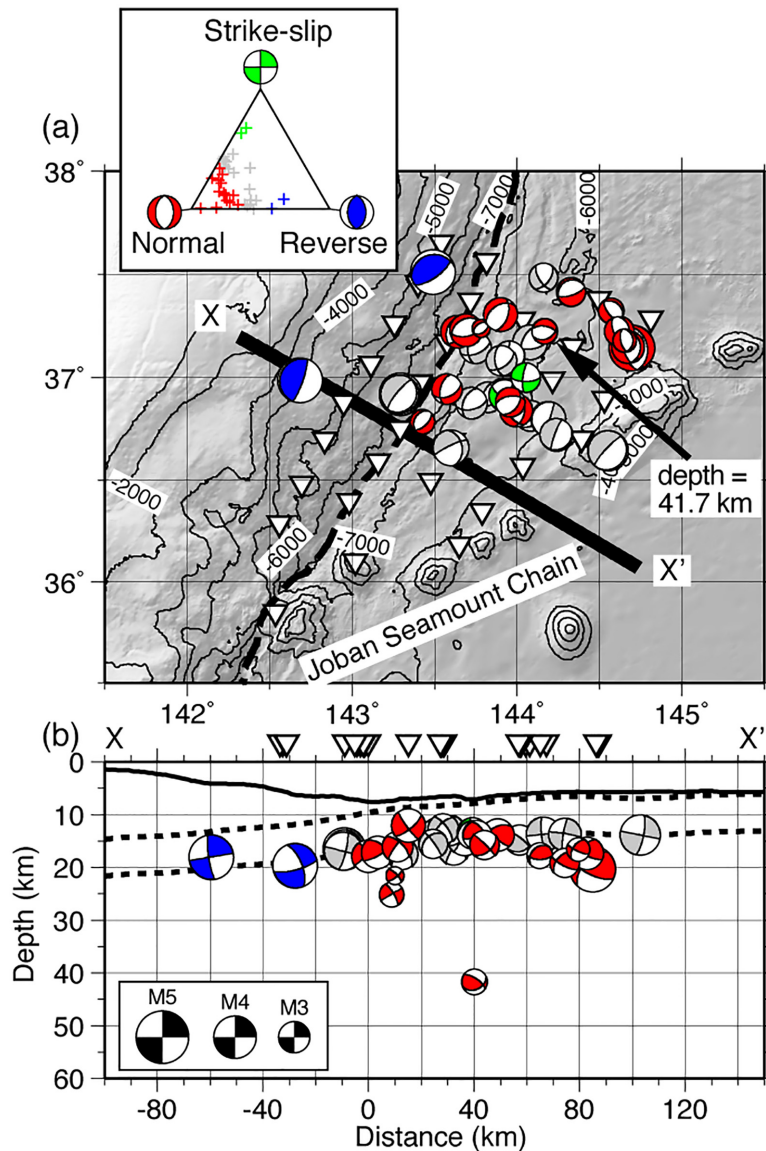


**Figure 4.** Focal mechanisms estimated from first-motion polarities of the OBS seismograms. (a) Map showing focal mechanisms. Focal mechanisms are colour-coded according to the triangle diagram of Frohlich (1992), which is presented in the inset panel. Red, blue, green and grey focal mechanisms indicate normal-faulting, reverse-faulting, strike-slip and other, respectively. The arrow points to the focal mechanism of the 41.7 km depth event. (b) Cross-section along X–X' profile on panel (a), which is the same as that in Fig. 3. Symbols are the same as Fig. 3(b).

suggesting a southern continuation of N–S striking normal-faults along a linear earthquake trend as observed previously (Obana *et al.* 2012, 2019), where the strike of the Japan Trench orients in the N–S direction (Fig. 5). However, the other two long linear earthquake trends (trend B and C) west of 144.5°E are roughly parallel to the trench axis in the southern Japan Trench. The *T*-axes of the earthquakes west of 144.5°E are generally normal to the trench axis of the southern Japan Trench.

Trench-parallel linear earthquake trends related to large intraplate normal-faulting earthquakes were observed in the previous OBS data along the Japan Trench. Examples are the aftershocks of the  $M_w$  7.4 intraplate normal-faulting earthquake 40 min after the 2011 Tohoku-oki earthquake (Obana *et al.* 2012), and two linear trends likely related to the aftershock activity of the 1933 Showa-Sanriku earthquake ( $M_w$  8.4, Obana *et al.* 2018). Although topographic structures associated with normal-faults in the trench-outer rise

region along the Japan Trench are divided into small segments oriented both parallel and oblique to the trench axis (Nakanishi 2011), the overall trends of the earthquake lineations roughly parallel to the trench axis extend over multiple segments. Hence, trench-parallel linear earthquake trends are possible indicators of the source faults of large intraplate normal-faulting earthquakes. Two linear earthquake trends (B and C in Fig. 5) parallel to the southern Japan Trench indicate the potential source faults of the normal-faulting earthquakes in the trench-outer rise region. In addition, the N–S striking linear earthquake trend A, which is the southward extension of the linear earthquake trend parallel to the northern Japan Trench, suggests that trench-parallel outer-rise normal-faults could lengthen even if the trench axis bends. In addition to the trench-parallel direction, strikes of the outer-rise normal-faults tend to orient in the direction parallel to abyssal hill fabrics, which are parallel to the magnetic lineations and orient ENE–WSW near the

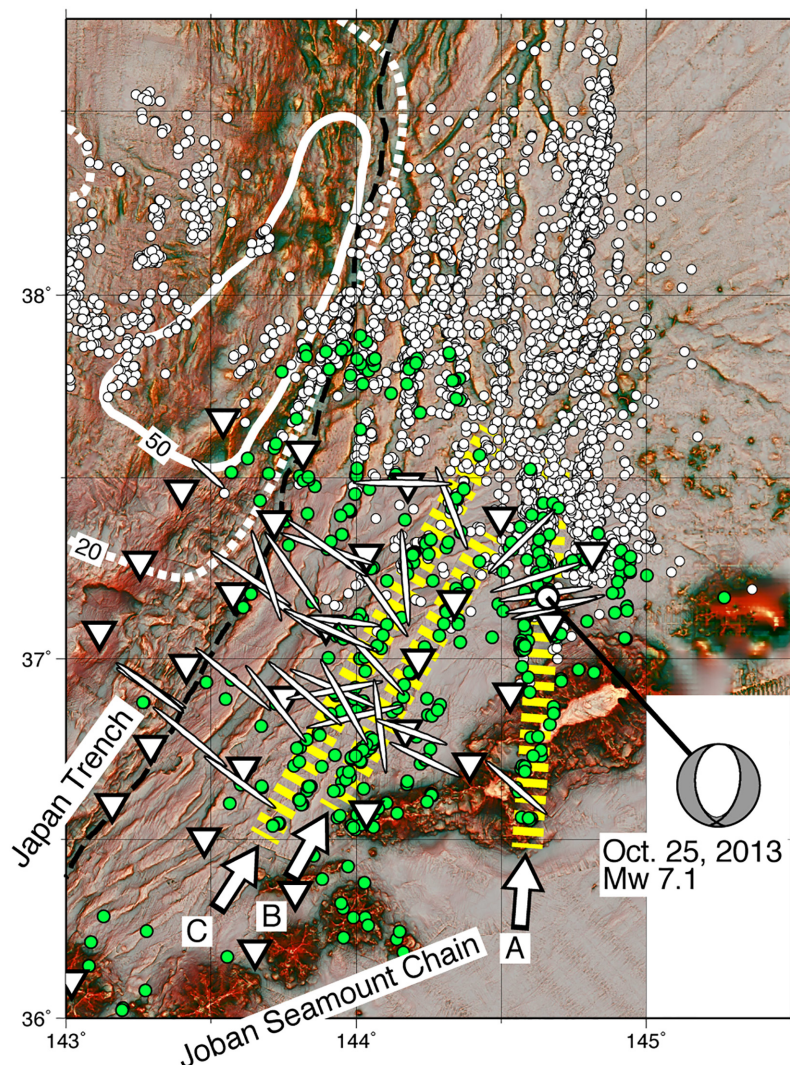


**Figure 5.** Red relief bathymetry map (Chiba *et al.* 2008) showing epicentre distribution and  $T$ -axes orientations seaward of the Japan Trench axis with a global CMT solution (Dziewonski *et al.* 1981; Ekström *et al.* 2012) of a  $M_w$  7.1 normal-faulting earthquake on 25 October 2013. The red relief map is designed to visualize both slope and convexity/concavity of topography using a combination of chroma and brightness in the red. Green and open circles are epicentres of the earthquakes shallower than 14 km obtained in this study and the previous study by Obana *et al.* (2019), respectively. Ellipsoids indicate orientations of the  $T$ -axes based on the focal mechanisms obtained in this study. Lengths of the axes correspond to plunge. The dashed black line indicates the Japan Trench axis. Dotted and solid white lines are the 20- and 50-m contours of coseismic slip distribution of the 2011 Tohoku-oki earthquake (Iinuma *et al.* 2012). Inverted triangles are the OBS locations. Arrows and yellow dotted lines indicate  $\sim 100$ -km-long linear earthquake trends (A–C).

Japan Trench (Billen *et al.* 2007; Nakanishi 2011). However, the trend A is not parallel to both. The trend A extends approximately  $\sim 100$  km southward beyond the bend of the trench axis. This length is equivalent to about one third to one half of the fault length of the 1933 Showa-Sanriku intraplate normal-faulting earthquake ( $M_w$  8.4, Kanamori 1971; Uchida *et al.* 2016). The strike of the faults is an important parameter to consider the tsunami hazard because propagation of the tsunami wave energy is concentrated in the direction perpendicular to the fault strike (e.g. Álvarez-Gómez *et al.* 2012). Therefore, such normal-faults oblique to the trench axis should be considered as substantial parts of large intraplate normal-faulting earthquakes.

Earthquakes in the oceanic mantle, which were observed mainly in the northern part of the OBS network, generally coincide with areas of lower  $V_p$  compared to surrounding regions (Fig. 6a). Many earthquakes were located near the 2013  $M_w$  7.1 and 2012  $M_w$  7.2

earthquakes, where the  $V_p$  in the oceanic mantle is relatively lower. Although these two  $M_7$ -class earthquakes occurred at the outer edge or outside of the OBS network, lower  $V_p$  areas around these two earthquakes are also imaged by the previous study in the central Japan Trench (Obana *et al.* 2019, fig. 12 therein). In addition, there is a low  $V_p$  area with mantle seismicity beneath the trench axis. The checkerboard resolution test using a trench-normal grid interval of 12.5 km shows that such linear velocity anomalies can be resolved (Fig. 6b). The low-velocity mantle is presumed to be relevant to faults in the oceanic mantle although the mechanisms of low velocities in the oceanic mantle in the trench-outer rise region, such as serpentinization caused by water infiltration through intraplate normal-faults (e.g. Ranero *et al.* 2003; Faccenda *et al.* 2009) or increase of crack-like water-filled porosities (Korenaga 2017), are still being discussed. The low  $V_p$  areas associated with the mantle seismicity suggest that the spatial heterogeneity in the

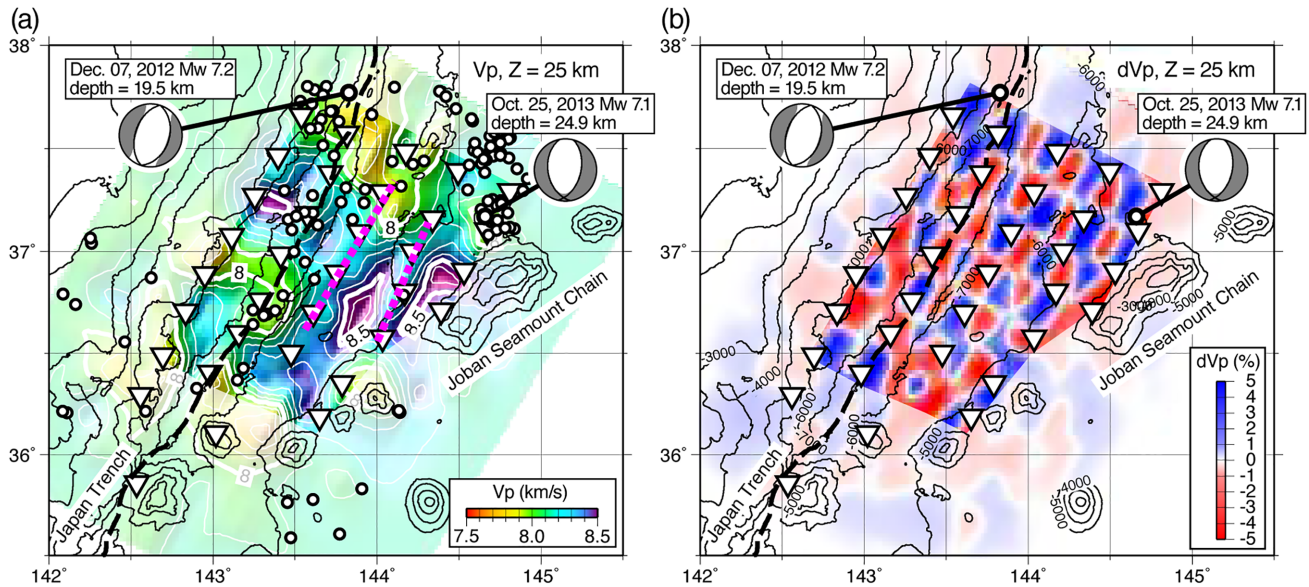


**Figure 6.**  $P$ -wave velocity ( $V_p$ ) and results of the checkerboard resolution test at a depth of 25 km. (a)  $V_p$  at a depth of 25 km and epicentres of the earthquakes at depths from 20 to 30 km (open circles). White lines are 0.1 km s<sup>-1</sup> interval contours of  $V_p$ . The velocity image is illuminated to highlight the spatial variations. The Global CMT solutions (Dziewonski *et al.* 1981; Ekström *et al.* 2012) of two M7-class earthquakes after the 2011 Tohoku-oki earthquakes (7 December 2012 and 25 October 2013) are indicated. Inverted triangles are the OBS locations. The dashed black line indicates the Japan Trench axis. Dotted purple lines are linear low  $V_p$  areas without mantle seismicity. Outside of the well-resolved area is masked based on the checkerboard resolution test shown in panel (b). (b) Results of the checkerboard resolution test for  $V_p$  at 25 km depth. The checkerboard grid interval normal to and parallel to the trench is 12.5 and 25 km, respectively.

uppermost oceanic mantle relates to the intraplate normal-faults extending into the oceanic mantle; these findings are similar to previous studies in central and northern Japan Trench (Obana *et al.* 2018, 2019). There are other linear low  $V_p$  trends (dotted purple lines in Fig. 6a). These low  $V_p$  areas may be an expression of intraplate normal-faults in the oceanic mantle although earthquakes within the oceanic mantle were not observed during our four months OBS observations.

## 5.2 Earthquakes beneath the trench landward slope

Previous OBS observations in the northern and central Japan Trench showed that there was almost no seismicity along the plate boundary or within the overriding plate beneath the trench landward slope north of 37.5°N (Obana *et al.* 2013, 2014, 2018). This aseismic wedge extends 40–50 km landward from the trench axis and coincides with the large coseismic slip of the 2011 Tohoku-oki earthquake and the source area of the 1896 Meiji-Sanriku Tsunami earthquake (Fig. 1). The OBS data in this study shows that the aseismic wedge continues southward, to approximately 37°N (Fig. 7). In contrast, earthquakes shallower than the subducting oceanic crust were observed beneath the trench landward slope south of 37°N. The differences in the hypocentre distribution of the earthquakes between the north and south of 37°N are apparent from the cross-sections along two profiles A–A' and B–B', even considering the location errors (Figs 7b and c). Hereafter, we refer to these two regions along the A–A' and B–B' profiles as the northern and southern regions, respectively.

Although the number of focal mechanisms obtained from the OBS observations in this study are limited, global CMT solutions (Dziewonski *et al.* 1981; Ekström *et al.* 2012) show along-trench variations in the focal mechanisms (Figs 7d–f). In the northern

region, global CMT solutions show normal-faulting focal mechanisms within ~30 km landward of the trench axis, as shown in the cross-section along A–A' (Fig. 7e). The hypocentre distribution obtained from the OBS observations and focal mechanisms of the global CMT solutions indicate that near-trench earthquakes landward of the trench axis in the northern region are intraplate normal-faulting earthquakes, as observed in the previous OBS observations farther north of the Japan Trench (Obana *et al.* 2013, 2014, 2018). Intraplate earthquakes were also observed within ~20 km landward of the trench axis along the B–B' profile in southern region (Fig. 7c). In addition, earthquakes apparently shallower than the intraplate earthquakes were located along the plate interface near the trench. Global CMT solutions show shallow reverse-faulting focal mechanisms near the trench in the southern region, as shown in the cross-section along B–B' (Fig. 7f). Although most of the global CMT solutions near the trench are located at a depth of 12 km, which is the minimum depth allowed for the centroid of the global CMT solutions (Ekström *et al.* 2012), these reverse-faulting earthquakes suggest that near-trench shallow seismicity in the southern region is different from the near-trench seismic activity to the north along the Japan Trench, which is characterized by the aseismic wedge and consists only of the intraplate normal-faulting earthquakes.

The area of the shallow near-trench reverse-faulting earthquakes coincide with the eastward (seaward) post-seismic movements, which indicate afterslip on the shallow plate interface (Tomita *et al.* 2017; Honsho *et al.* 2019, Fig. 7a). Furthermore, the episodic activities of tectonic tremors with reverse-faulting focal mechanisms were reported by Ohta *et al.* (2019) from the OBS observations conducted in the area adjacent to this study. The shallow near-trench earthquakes are in the surrounding region of the tremor activities, including seaward of tremors close to the trench axis (Figs 7a and c).

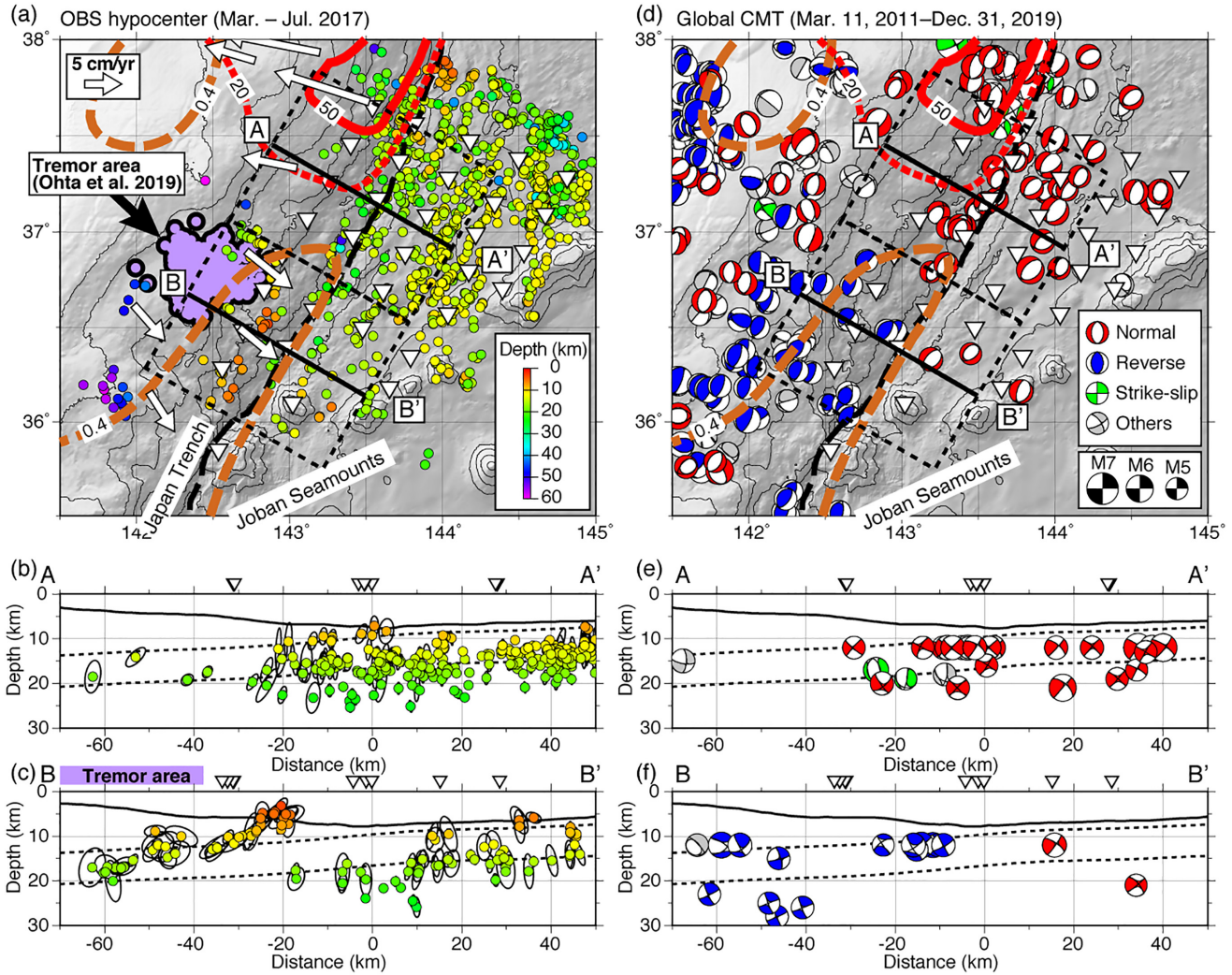


**Figure 7.** Hypocentre distribution obtained from the OBS observations and the global CMT solutions near the trench axis. (a) Map showing hypocentre distribution. The hypocenters are colour-coded by their depth. Dashed line is the Japan Trench axis. Inverted triangles are the OBS locations. Arrows are horizontal displacement rates relative to the North American Plate (Honsho *et al.* 2019). Purple area indicates the tremor activity area based on the OBS observations by Ohta *et al.* (2019). Dotted and solid red lines are the 20- and 50-m contours of coseismic slip distribution of the 2011 Tohoku-oki earthquake (Iinuma *et al.* 2012). Dashed brown contours indicate afterslip distribution of the 2011 Tohoku-oki earthquake at 0.4-m intervals (Iinuma *et al.* 2016). (b, c) Hypocentre distribution and error ellipsoids projected onto the cross-sections along two profiles, A–A' (b) and B–B' (c) indicated by thick solid lines on panel (a). Events within the dotted rectangles are indicated on each panel. Purple bar at the top of the panel (c) is the projected range of the tremor activity area (Ohta *et al.* 2019). Dotted lines roughly correspond to the top of the oceanic crust and oceanic Moho (as in Fig. 3b). Inverted triangles indicate OBS locations projected onto each profile (plotted at the top of the panel regardless of water depth). (d) Global CMT solutions (Dziewonski *et al.* 1981; Ekström *et al.* 2012) of events larger than  $M_w$  5.0 after the 2011 Tohoku-oki Earthquake to December 2019. The CMT solutions are colour-coded by mechanism type according to Frohlich (1992). (e, f) Global CMT solutions projected onto the cross-sections along two profiles, A–A' (e) and B–B' (f) indicated by thick lines on panel (d). The CMT solutions within the dotted rectangles are indicated on each panel.

The shallow near-trench earthquake activities correlate with the episodic tremor activities in time, as opposed to the earthquakes seaward of the trench, which do not show any significant correlation with the tremor episodes (Fig. 8b). During our OBS observations from March to July 2017, two tremor episodes in March and May were reported. The migration of those tremor activities along the trench-parallel direction is explained by parabola curves with a diffusive coefficient of  $1.5 \times 10^3 \text{ m}^2\text{s}^{-1}$  (Ohta *et al.* 2019). The near-trench earthquakes observed by our OBSs can be explained as activity correlating with the tremor episodes, with the parabolas of the same diffusive coefficient along the directions both parallel and normal to the trench (Figs 8c–f). The episodic tremor activity is likely related to the intermittent slow slip events in the afterslip area

on the shallow plate interface near the trench (Ohta *et al.* 2019). Even though the analysis using seafloor geodetic measurements cannot constrain the seaward extent of the afterslip to the trench axis (Iinuma *et al.* 2016), the shallow near-trench earthquakes correlated with the tremor activity, suggesting that the afterslip on the plate interface extended episodically close to the trench axis and generated shallow near-trench earthquakes.

### 5.3 Structure variations and slip behaviours in the shallow subduction zone

The Joban seamount chain is in the trench seaward slope (Fig. 9a) and previous active seismic studies have imaged subducted

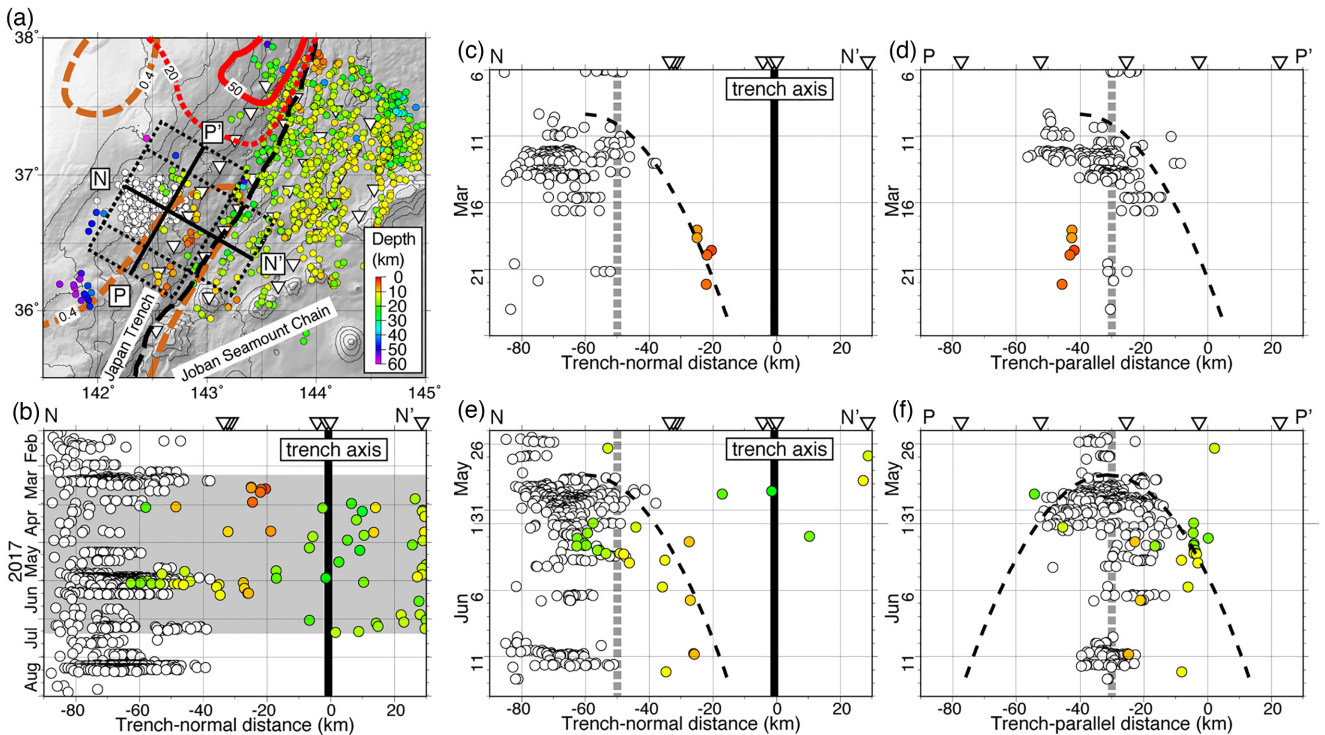


**Figure 8.** Map and space-time plots of earthquake and tremor activity. (a) Map showing distribution of the earthquakes observed in this study (circles colour-coded by depth) and tremors (open circles) observed by Ohta *et al.* (2019). Dotted and solid red lines, dashed brown and black lines, and inverted triangles are the same as those in Fig. 7. (b) Space-time plot of the earthquakes and tremors along the trench-normal profile N–N' indicated by thick solid black line in panel (a). Colour and open circles are the same as in panel (a). Events within the dotted rectangle are indicated. Thick vertical line indicates the location of the trench axis. Grey shaded period corresponds to the OBS observations of this study. Inverted triangles indicate the OBS locations projected onto the profile. (c, d) Space-time plots along trench-normal profile N–N' (c) and trench-parallel profile P–P' (d) for 20 d from 6 March 2017. Events within the dotted rectangles are indicated on each panel. Dashed parabola calculated using the diffusion coefficient of  $1.5 \times 10^3 \text{ m}^2 \text{ s}^{-1}$ . Dotted grey vertical lines indicate the intersection of two profiles. (e, f) Space-time plots along the profile N–N' (e) and P–P' (f) for 20 d from 25 May 2017.

seamounts in the southern Japan Trench (Mochizuki *et al.* 2008; Nishizawa *et al.* 2009). Although the Joban seamount chain intersects the Japan Trench at approximately  $36^\circ\text{N}$  and the subducted seamount has been imaged south of  $36^\circ\text{N}$ , the elongated channel-like low-velocity sedimentary units along the plate interface, which are presumed to relate with the subducted seamounts, have been imaged by multichannel seismic surveys on profiles across the trench south of  $37.5^\circ\text{N}$  (Tsuru *et al.* 2002; Kodaira *et al.* 2017, Fig. 9a). In particular, the low-velocity units thicker than 1 km have been imaged along the seismic profiles perpendicular to the trench south of  $37^\circ\text{N}$ . In contrast, a prism-shaped low-velocity wedge (frontal prism) has been imaged at the toe of the overriding plate along the profiles north of  $37.5^\circ\text{N}$  (Tsuru *et al.* 2002; Kodaira *et al.* 2017). In addition, the upper plate structure boundary (forearc segment boundary), mapped by Bassett *et al.* (2016), coincides with the boundary between the channel-like low-velocity unit and the frontal prism (Fig. 9a). These large-scale structure variations along the Japan Trench roughly correlate with the differences in the co- and post-seismic deformations of the 2011 Tohoku-oki earthquake between central and southern Japan Trench. While the large coseismic slip over 50 m during the 2011 Tohoku-oki earthquake and westward post-seismic deformations were observed to the north, eastward post-seismic deformations, suggesting shallow afterslip near the trench, were observed to the south (Fig. 9a). The along-trench structure variations are supposed to be a primary factor controlling the seismogenic behaviour along the plate interface (Bassett *et al.* 2016; Kodaira *et al.* 2017).

The OBS observations in this study detected near-trench shallow earthquakes correlated with the episodic tremors south of the large-scale structure boundary, where the eastward post-seismic deformations were observed (Tomita *et al.* 2017; Honsho *et al.* 2019, Fig. 9a). The near-trench earthquakes are regular earthquakes, of which both *P*- and *S*-wave arrivals are evident on the seismograms recorded by the OBSs with short-period seismometers (Fig. S4), and are different from the tectonic tremors observed by Ohta *et al.* (2019). The results from the OBS observations in the southern Japan Trench by Ohta *et al.* (2019) and this study indicate proximity between slow slip events and regular earthquakes in shallow subduction zones near the trench (Figs 9a and c). Nishikawa *et al.* (2019) has pointed out that the tremors in the southern Japan Trench, which occur very close to the earthquake swarms and repeating earthquakes, are different from those in other subduction zones based on the continuous seismic data obtained by the seafloor cable observation network which runs along the entire Japan Trench. The near-trench regular earthquakes near the slow slip events are a distinctive feature of the seismic activity in the southern Japan Trench.

Besides the large-scale along-trench structure variation, seismic reflection surveys revealed the heterogeneous distribution of the channel-like low-velocity sedimentary unit in the southern Japan Trench (Tsuru *et al.* 2002, Fig. 9a). The thickness of the low-velocity unit varies with profiles from hundreds of metres to 2 km. In addition, a 10-km-scale variation in the thickness of the low-velocity unit, which is on the order comparable to the seamounts belonging to the Joban seamount chain, have been imaged along the profiles

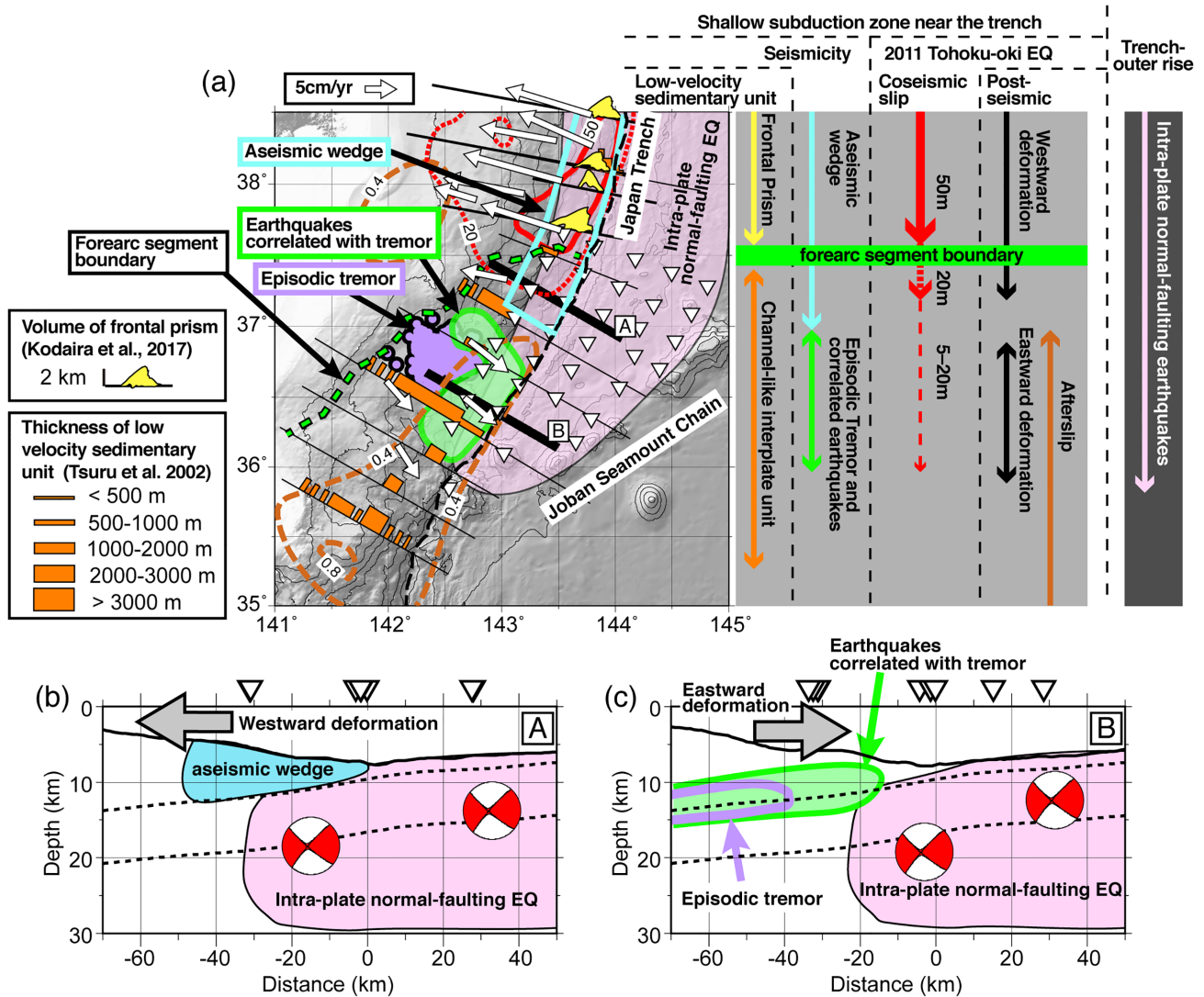


**Figure 9.** Summary of along-trench variations in earthquake activity, co- and post-seismic deformation, and structural features. (a) Map showing the areas of episodic tremor, near-trench earthquakes correlated with the tremor, and aseismic wedge. Purple and green area indicates the region of the episodic tremor (Ohta *et al.* 2019) and earthquakes correlated with the tremor observed in this study, respectively. Light blue rectangle is the area of the aseismic wedge from this study and Obana *et al.* (2013). Arrows, dotted and solid red lines, dashed brown and black lines and inverted triangles are the same as those in Fig. 7. Dashed green line is the forearc segment boundary in upper plate structure (Bassett *et al.* 2016). The distribution of low-velocity sedimentary units inferred from seismic reflection surveys along the black lines are shown. Brown bars are the thickness of low velocity sedimentary unit (Tsuru *et al.* 2002), and yellow areas are the volume of the low-velocity frontal prism (Kodaira *et al.* 2017). Light pink areas indicate the area of intraplate normal-faulting earthquakes from this study and previous studies (Asano *et al.* 2011; Nakamura *et al.* 2016; Obana *et al.* 2019). Note that the OBS observations in this study were conducted north of Joban seamount chain and southern bound of the intraplate normal-faulting activity indicated in this figure does not indicate there are no intraplate normal-faulting earthquakes farther south. The right panel indicates the summary of the along-trench variations. In addition to the areas with the coseismic slip over 50 m and 20 m by Iinuma *et al.* (2012) that are indicated in the map, the area with 5–20 m coseismic slip near the trench (e.g. Ide *et al.* 2011; Shao *et al.* 2011; Blettery *et al.* 2014) is indicated by the red dashed arrow. (b, c) Schematic cross-section along the profiles, A (b) and B (c) indicated by thick solid lines on panel (a). These profiles are the same with the profiles shown in Fig. 7.

parallel to the trench (Tsuru *et al.* 2002). Similar 10–15 km wide seamount-scale structure heterogeneity was imaged along the profiles perpendicular to the trench at the Ecuador margin, where the Carnegie Ridge enters the subduction zone (Sage *et al.* 2006). The structural heterogeneity of the channel-like sedimentary units could cause seamount-scale variations in the interplate coupling (Tsuru *et al.* 2002; Sage *et al.* 2006). Such structural heterogeneities on the plate interface are likely related to the smaller spatial scale variations in the slip behaviours in southern Japan Trench, resulting in the proximity between the slow slips and the regular earthquakes.

Although the large-scale along-trench structure variation is a primary factor controlling seismogenic behaviour, the aseismic wedge coincident with the large (>50 m) coseismic slip of the 2011 Tohoku-oki earthquake and 1896 Meiji-Sanriku Tsunami earthquake rupture (Obana *et al.* 2013, 2018, Fig. 1) extends southward to approximately 37°N, beyond the large-scale structure boundary (Figs 9a and b). In addition, several studies have reported that the coseismic rupture area with 5–20 m slip near the trench extends southward to 36° to 36.5°N (Ide *et al.* 2011; Shao *et al.* 2011; Blettery *et al.* 2014). Near-surface rupture on the shallow megathrust interface close to the trench activate normal-faulting earthquakes

in the trench-outer rise region (Sato *et al.* 2012; Sladen & Trevisan 2018). Considering the area of the intraplate normal-faulting earthquakes in the trench-outer rise region extending southward to 36°N, as reported from onshore observations (Asano *et al.* 2011; Nakamura *et al.* 2016) and observed in this study (Figs 3 and 9a), the coseismic rupture of the 2011 Tohoku-oki earthquake might slip into the afterslip area estimated by Iinuma *et al.* (2016), where seafloor geodetic measurements show eastward movements (Tomita *et al.* 2017; Honsho *et al.* 2019). If so, near-trench shallow plate interface in southern Japan Trench host both the coseismic rupture and the post-seismic slow slip of the 2011 Tohoku-oki earthquake. Relationships between the smaller spatial scale structure variations and frictional properties on the plate interface would be a key to understanding the diverse slip behaviours in the shallow subduction zone of the southern Japan Trench.

## 6 CONCLUSIONS

We conducted four months of earthquake observations in the southern Japan Trench off Ibaraki and Fukushima using OBSs and obtained detailed earthquake distributions for both the seaward and landward slopes south of the main rupture area of the 2011 Tohoku-oki earthquake. Hypocentres and focal mechanisms were estimated based on the 3-D seismic velocity structure.

Normal-faulting earthquakes in the trench-outer rise region were observed to be similar to the trench-outer rise region of the main rupture area of the 2011 Tohoku-oki earthquake. The seismicity in the trench-outer rise region continued southward to 36°N at least. Although it is difficult to evaluate the extent of depth of the extensional stress regime within the Pacific Plate due to the limited number of focal mechanisms for events at deeper depths, the OBS data supports the activation of the normal-faulting earthquakes following the 2011 Tohoku-oki earthquake, as reported from onshore seismic observations. The earthquakes located seaward of the trench axis show three ~100-km-long linear trends. Two of them are parallel to the trench axis in the southern Japan Trench. The other one, which is oblique to the trench axis, is a southern extension of the trench-parallel linear earthquake trend in the central Japan Trench. Although the strike of the southern Japan Trench is different by approximately 20° from that of the central to northern Japan Trench, the observed linear trend suggests that the trench-parallel normal-faults within the incoming Pacific Plate extend linearly beyond the bend of the trench. This indicates that the potential of the normal-faults oblique to the trench axis can be considered to be a part of the large intraplate normal-faulting earthquakes and related tsunamis.

In the trench landward slope, an aseismic wedge, where few earthquakes occurred on the plate interface and within the over-riding plates, was observed north of 37°N, similar to the north of the Japan Trench. In contrast, shallow near-trench earthquakes were observed south of 37°N. The contrast of the near-trench seismicity landward of the trench axis correlates with the along-trench variations in the direction of the post-seismic deformations obtained from the seafloor geodetic measurements. Based on the correlation of the shallow near-trench earthquakes with the episodic tremor activities in the afterslip area, afterslip likely extended close to the trench axis. Large-scale along-trench structure variations, such as the low-velocity sedimentary unit and over-riding plate structure, is a primary factor controlling the variations in the co- and post-seismic behaviour between the central and southern Japan Trench. In addition, seamount-scale structure

heterogeneities in the channel-like low-velocity interplate sedimentary unit will likely affect the seismogenic behaviour in shallow subduction zone of the southern Japan Trench, which is characterized by diverse slip behaviours with proximity of the slow slips and regular earthquakes.

Detailed hypocentre distribution can illuminate the temporal and spatial evolution of slips in shallow subduction zones. Although horizontal separation between the OBSs used in this study, they were not enough to constrain the hypocentres for such shallow earthquakes. Future comparisons of both the precise hypocentres and the focal mechanisms with the detailed crustal structures would provide important insights into the relationships between crustal structures and diverse slip behaviours in the shallow subduction zone.

## ACKNOWLEDGEMENTS

This work was supported by JSPS KAKENHI Grant Numbers JP15H05718 and JP16H04045. We are grateful to the captains and crews of R/V *Kairei* for their kind support during the cruises. We would like to thank Ryota Hino, Masanao Shinohara, Kazuaki Ohta and Takeshi Iinuma for their discussions. Bathymetry data by Kido *et al.* (2011), JHOD & JAMSTEC (2011) and Olson *et al.* (2016) were used to prepare the red relief map. We also thank Stuart Henrys, Sylvain Barbot and editor Jenny Collier for their constructive comments.

## DATA AVAILABILITY

The OBS data underlying this article will be available in JAMSTEC Seismic Survey Database, at <https://doi.org/10.17596/0002069>. The tremor catalogue by Ohta *et al.* (2019) was obtained from <https://doi.org/10.1029/2019GL082468>. The Global CMT catalogue (Dziewonski *et al.* 1981; Ekström *et al.* 2012) is available at <https://www.globalcmt.org>.

## REFERENCES

- Agata, R., Barbot, S.D., Fujita, K., Hyodo, M., Iinuma, T., Nakata, R., Ichimura, T. & Hori, T., 2019. Rapid mantle flow with power-law creep explains deformation after the 2011 Tohoku mega-quake, *Nat. Commun.*, **10**(1), 1385, doi: 10.1038/s41467-019-08984-7.
- Aki, K., 1965. 17. Maximum likelihood estimate of  $b$  in the formula  $\log N = a - bM$  and its confidence limits, *Bull. Earthq. Res. Inst.*, **43**, 237–239.
- Álvarez-Gómez, J.A., Gutiérrez, O.Q., Aniel-Quiroga, C. & González, M., 2012. Tsunamigenic potential of outer-rise normal faults at the Middle America trench in Central America, *Tectonophysics*, **574–575**, 133–143.
- Argus, D.F., Gordon, R.G. & DeMets, C., 2011. Geologically current motion of 56 plates relative to the no-net-rotation reference frame, *Geochem. Geophys. Geosyst.*, **12**, 11, doi:10.1029/2011GC003751.
- Asano, Y., Saito, T., Ito, Y., Shiomi, K., Hirose, H., Matsumoto, T., Aoi, S., Hori, S. & Sekiguchi, S., 2011. Spatial distribution and focal mechanisms of aftershocks of the 2011 off the Pacific coast of Tohoku Earthquake, *Earth Planets Space*, **63**(7), 669–673.
- Barbot, S., 2020. Frictional and structural controls of seismic super-cycles at the Japan trench, *Earth, Planets Space*, **72**(1), 63, doi: 10.1186/s40623-020-01185-3.
- Bassett, D., Sandwell, D.T., Fialko, Y. & Watts, A.B., 2016. Upper-plate controls on co-seismic slip in the 2011 magnitude 9.0 Tohoku-oki earthquake, *Nature*, **531**(7592), 92–96.
- Billen, M., Cowgill, E. & Buer, E., 2007. Determination of fault friction from reactivation of abyssal-hill faults in subduction zones, *Geology*, **35**(9), 819–822.

- Bletery, Q., Sladen, A., Delouis, B., Vallée, M., Nocquet, J.-M., Rolland, L. & Jiang, J., 2014. A detailed source model for the Mw9.0 Tohoku-Oki earthquake reconciling geodesy, seismology, and tsunami records, *J. geophys. Res.*, **119**(10), 7636–7653.
- Chiba, T., Kaneta, S.-I. & Suzuki, Y., 2008. Red relief image map: new visualization method for three dimensional data, *The International Archives of the Photogrammetry, Remote Sensing and Spatial Information Sciences*, **37**(B2), 1071–1076.
- Dzieweński, A.M., Chou, T.-A. & Woodhouse, J.H., 1981. Determination of earthquake source parameters from waveform data for studies of global and regional seismicity, *J. geophys. Res.*, **86**(B4), 2825–2852.
- Ekström, G., Nettles, M. & Dzieweński, A., 2012. The global CMT project 2004–2010: Centroid-moment tensors for 13,017 earthquakes, *Phys. Earth planet. Inter.*, **200–201**, 1–9.
- Faccenda, M., Gerya, T.V. & Burlini, L., 2009. Deep slab hydration induced by bending-related variations in tectonic pressure, *Nat. Geosci.*, **2**(11), 790–793.
- Frohlich, C., 1992. Triangle diagrams: ternary graphs to display similarity and diversity of earthquake focal mechanisms, *Phys. Earth planet. Inter.*, **75**(1–3), 193–198.
- Fujie, G., Kodaira, S., Nakamura, Y., Obana, K. & Miura, S., 2019. Spatial variations in incoming oceanic plate and its implications for subduction zone processes along the Japan Trench, *Abstract T41C-01, presented at 2019 Fall Meeting, AGU, San Francisco, CA*.
- Fujiwara, T., Kodaira, S., No, T., Kaiho, Y., Takahashi, N. & Kaneda, Y., 2011. The 2011 Tohoku-Oki earthquake: displacement reaching the trench axis, *Science*, **334**(6060), 1240–1240.
- Hardebeck, J.L. & Shearer, P.M., 2002. A new method for determining first-motion focal mechanisms, *Bull. seism. Soc. Am.*, **92**, 2264–2276.
- Hino, R. et al., 2009. Insight into complex rupturing of the immature bending normal fault in the outer slope of the Japan Trench from aftershocks of the 2005 Sanriku earthquake (Mw = 7.0) located by ocean bottom seismometry, *Geochem. Geophys. Geosyst.*, **10**(7), Q07O18, doi:10.1029/2009GC002415.
- Hirata, N. & Matsu'ura, M., 1987. Maximum-likelihood estimation of hypocenter with origin time eliminated using nonlinear inversion technique, *Phys. Earth planet. Inter.*, **47**, 50–61.
- Honsho, C., Kido, M., Tomita, F. & Uchida, N., 2019. Offshore post-seismic deformation of the 2011 Tohoku earthquake revisited: application of an improved GPS-acoustic positioning method considering horizontal gradient of sound speed structure, *J. geophys. Res.*, **124**(6), 5990–6009.
- Ide, S., Baltay, A. & Beroza, G.C., 2011. Shallow dynamic overshoot and energetic deep rupture in the 2011 Mw 9.0 Tohoku-Oki earthquake, *Science*, **332**(6036), 1426–1429.
- Inuma, T. et al., 2012. Coseismic slip distribution of the 2011 off the Pacific Coast of Tohoku Earthquake (M9.0) refined by means of seafloor geodetic data, *J. geophys. Res.*, **117**(B7), B07409, doi:10.1029/2012JB009186.
- Inuma, T., Hino, R., Uchida, N., Nakamura, W., Kido, M., Osada, Y. & Miura, S., 2016. Seafloor observations indicate spatial separation of coseismic and postseismic slips in the 2011 Tohoku earthquake, *Nat. Commun.*, **7**(1), 13506, doi: 10.1038/ncomms13506.
- Ito, A., Fujie, G., Miura, S., Kodaira, S., Kaneda, Y. & Hino, R., 2005. Bending of the subducting oceanic plate and its implication for rupture propagation of large interplate earthquakes off Miyagi, Japan, in the Japan Trench subduction zone, *Geophys. Res. Lett.*, **32**, L05310, doi: 10.1029/2004GL022307.
- JHOD, JAMSTEC, 2011. Bathymetry data off Tohoku, Japan, *Seismol. Soc. Jpn., News Lett.*, **23**(2), 35–36 (in Japanese).
- Kanamori, H., 1971. Seismological evidence for a lithospheric normal faulting—the Sanriku earthquake of 1933, *Phys. Earth planet. Inter.*, **4**, 289–300.
- Kido, Y., Fujiwara, T., Sasaki, T., Kinoshita, M., Kodaira, S., Sano, M., Yasunori Hanafusa, Y.I. & Tsuboi, S., 2011. Bathymetric feature around Japan Trench obtained by JAMSTEC multi narrow beam survey, in *MIS026-P58, presented at Japan Geoscience Union Meeting 2011*, Chiba, Japan.
- Kodaira, S. et al., 2017. Depth-varying structural characters in the rupture zone of the 2011 Tohoku-oki earthquake, *Geosphere*, **13**(5), 1408–1424.
- Korenaga, J., 2017. On the extent of mantle hydration caused by plate bending, *Earth Planet. Sci. Lett.*, **457**, 1–9.
- Lay, T., Ammon, C., Kanamori, H., Kim, M. & Xue, L., 2011. Outer trench-slope faulting and the 2011 Mw 9.0 off the Pacific coast of Tohoku Earthquake, *Earth Planets Space*, **63**(7), 713–718.
- Maeda, Y., Asakawa, K., Obana, K. & Terada, I., 2013. Super-deep-sea ocean bottom seismometers using ceramic spheres, in *Proceedings of the 2013 IEEE International Underwater Technology Symposium (UT)*, 1–4, pp. doi: 10.1109/UT.2013.6519902.
- Mizuno, M., Sato, T., Shinohara, M., Mochizuki, K., Yamada, T. & Kanazawa, T., 2009. Seismicity in the seaward slope of the Japan Trench, off Ibaraki, using ocean bottom seismometers for long-term observation, *Zisin (J. Seismol. Soc. Jpn.)*, **62**(1), 19–23 (in Japanese).
- Mochizuki, K., Yamada, T., Shinohara, M., Yamanaka, Y. & Kanazawa, T., 2008. Weak interplate coupling by seamounts and repeating M 7 earthquakes, *Science*, **321**(5893), 1194–1197.
- Nakamura, W., Uchida, N. & Matsuzawa, T., 2016. Spatial distribution of the faulting types of small earthquakes around the 2011 Tohoku-oki earthquake: a comprehensive search using template events, *J. geophys. Res.*, **121**(4), 2591–2607.
- Nakamura, Y. et al., 2014. Seismic imaging and velocity structure around the JFAST drill site in the Japan Trench: low Vp, high Vp/Vs in the transparent frontal prism, *Earth Planets Space*, **66**(1), 121, doi:10.1186/1880-5981-66-121.
- Nakanishi, M., 2011. Bending-related topographic structures of the subducting plate in the northwestern Pacific Ocean: accretionary prisms and convergent margin tectonics in the northwest Pacific basins, in *Modern Approaches in Solid Earth Sciences*, Vol. **8**, pp. 1–38, eds Ogawa, Y., Anma, R. & Dilek, Y., Springer Netherlands.
- Nishikawa, T., Matsuzawa, T., Ohta, K., Uchida, N., Nishimura, T. & Ide, S., 2019. The slow earthquake spectrum in the Japan Trench illuminated by the S-net seafloor observatories, *Science*, **365**(6455), 808–813.
- Nishizawa, A., Kaneda, K., Watanabe, N. & Oikawa, M., 2009. Seismic structure of the subducting seamounts on the trench axis: Erimo Seamount and Daiichi-Kashima Seamount, northern and southern ends of the Japan Trench, *Earth Planets Space*, **61**(3), e5–e8.
- Obana, K., Fujie, G., Takahashi, T., Yamamoto, Y., Nakamura, Y., Kodaira, S., Takahashi, N., Kaneda, Y. & Shinohara, M., 2012. Normal-faulting earthquakes beneath the outer slope of the Japan Trench after the 2011 Tohoku earthquake: implications for the stress regime in the incoming Pacific plate, *Geophys. Res. Lett.*, **39**, L00G24, doi:10.1029/2011GL050399.
- Obana, K. et al., 2013. Aftershocks near the updip end of the 2011 Tohoku-Oki earthquake, *Earth planet. Sci. Lett.*, **382**, 111–116.
- Obana, K., Kodaira, S., Nakamura, Y., Sato, T., Fujie, G., Takahashi, T. & Yamamoto, Y., 2014. Aftershocks of the December 7, 2012 intraplate doublet near the Japan Trench axis, *Earth Planets Space*, **66**(1), 1–6.
- Obana, K., Nakamura, Y., Fujie, G., Kodaira, S., Kaiho, Y., Yamamoto, Y. & Miura, S., 2018. Seismicity in the source areas of the 1896 and 1933 Sanriku earthquakes and implications for large near-trench earthquake faults, *Geophys. J. Int.*, **212**(3), 2061–2072.
- Obana, K., Fujie, G., Takahashi, T., Yamamoto, Y., Tonegawa, T., Miura, S. & Kodaira, S., 2019. Seismic velocity structure and its implications for oceanic mantle hydration in the trench-outer rise of the Japan Trench, *Geophys. J. Int.*, **217**(3), 1629–1642.
- Ohta, K., Ito, Y., Hino, R., Ohyanagi, S., Matsuzawa, T., Shiobara, H. & Shinohara, M., 2019. Tremor and inferred slow slip associated with afterslip of the 2011 Tohoku Earthquake, *Geophys. Res. Lett.*, **46**(9), 4591–4598.
- Olson, C.J., Becker, J.J. & Sandwell, D.T., 2016. SRTM15 PLUS: data fusion of Shuttle Radar Topography Mission (SRTM) land topography with measured and estimated seafloor topography (NCEI Accession 0150537), *NOAA National Centers for Environmental Information*, Available

- at: <https://www.ncei.noaa.gov/archive/accession/0150537>, Accessed 9 February 2021.
- Ranero, C.R., Morgan, J.P., McIntosh, K. & Reichert, C., 2003. Bending-related faulting and mantle serpentinization at the Middle America trench, *Nature*, **425**, 367–373.
- Sage, F., Collot, J.-Y. & Ranero, C., 2006. Interplate patchiness and subduction-erosion mechanisms: evidence from depth-migrated seismic images at the central Ecuador convergent margin, *Geology*, **34**(12), 997–1000.
- Sathiakumar, S., Barbot, S.D. & Agram, P., 2017. Extending resolution of fault slip with geodetic networks through optimal network design, *J. geophys. Res.*, **122**(12), 10538–10558.
- Sato, T., Hiratsuka, S. & Mori, J., 2012. Coulomb stress change for the normal-fault aftershocks triggered near the Japan Trench by the 2011 Mw 9.0 Tohoku-Oki earthquakes, *Earth Planets Space*, **64**, doi: 10.5047/eps.2012.04.003.
- Shao, G., Li, X., Ji, C. & Maeda, T., 2011. Focal mechanism and slip history of the 2011 Mw 9.1 off the Pacific coast of Tohoku Earthquake, constrained with teleseismic body and surface waves, *Earth Planets Space*, **63**(7), 559–564.
- Shinohara, M., Hino, R., Yoshizawa, T., Nishino, M., Sato, T. & Suyehiro, K., 2005. Hypocenter distribution of plate boundary zone off Fukushima, Japan, derived from ocean bottom seismometer data, *Earth Planets Space*, **57**(2), 93–105.
- Shinohara, M. *et al.*, 2012. Precise aftershock distribution of the 2011 off the Pacific coast of Tohoku earthquake revealed by ocean bottom seismometer networks, *Earth Planets Space*, **64**(12), 1137–1148.
- Sladen, A. & Trevisan, J., 2018. Shallow megathrust earthquake ruptures betrayed by their outer-trench aftershocks signature, *Earth planet. Sci. Lett.*, **483**, 105–113.
- Sun, T. & Wang, K., 2015. Viscoelastic relaxation following subduction earthquakes and its effects on afterslip determination, *J. geophys. Res.*, **120**(2), 1329–1344.
- Sun, T. *et al.*, 2014. Prevalence of viscoelastic relaxation after the 2011 Tohoku-oki earthquake, *Natures*, **514**(7520), 84–87.
- Sun, T., Saffer, D. & Ellis, S., 2020. Mechanical and hydrological effects of seamount subduction on megathrust stress and slip, *Nat. Geosci.*, **13**(3), 249–255.
- Tanioka, Y. & Satake, K., 1996. Fault parameters of the 1896 Sanriku tsunami earthquake estimated from tsunami numerical modeling, *Geophys. Res. Lett.*, **23**(13), 1549–1552.
- Tomita, F., Kido, M., Ohta, Y., Iinuma, T. & Hino, R., 2017. Along-trench variation in seafloor displacements after the 2011 Tohoku earthquake, *Sci. Adv.*, **3**(7), doi: 10.1126/sciadv.1700113.
- Tsuru, T., Park, J.-O., Miura, S., Kodaira, S., Kido, Y. & Hayashi, T., 2002. Along-arc structural variation of the plate boundary at the Japan Trench margin: implication of interplate coupling, *J. geophys. Res.*, **107**, 2357.
- Uchida, N., Kirby, S.H., Umino, N., Hino, R. & Kazakami, T., 2016. The great 1933 Sanriku-oki earthquake: reappraisal of the main shock and its aftershocks and implications for its tsunami using regional tsunami and seismic data, *Geophys. J. Int.*, **206**(3), 1619–1633.
- Urabe, T. & Tsukada, S., 1992. win-A workstation program for processing waveform data from microearthquake networks, Programme and Abstracts, *Seismol. Soc. Jpn.*, **2**, pp. 331.
- Utsu, T., 1965. A method for determining the value of  $b$  in a formula  $\log n = a - bm$  showing the magnitude-frequency relation for earthquakes, *Geophys. Bull. Hokkaido Univ.*, **13**(99), 103, doi:10.14943/gbhu.13.99.
- Watanabe, H., 1971. Determination of earthquake magnitude at regional distance in and near Japan, *Zisin (J. Seismol. Soc. Jpn.)*, **24**, 189–200 (in Japanese with English abstract).
- Yagi, Y. & Fukahata, Y., 2011. Rupture process of the 2011 Tohoku-oki earthquake and absolute elastic strain release, *Geophys. Res. Lett.*, **38**(19), L19307, doi:10.1029/2011GL048701.
- Zhang, H. & Thurber, C.H., 2003. Double-difference tomography: the method and its application to the Hayward Fault, California, *Bull. seism. Soc. Am.*, **93**(5), 1875–1889.

## SUPPORTING INFORMATION

Supplementary data are available at [GJI](#) online.

**Figure S1.** Initial model of the double-difference tomography analysis. (a) Map showing the initial  $V_p$  velocity model at a depth of 20 km. The crosses indicate grid nodes of the velocity model. The inverted triangles are the OBS locations. The red solid and dashed lines are the survey line of A6 (Fujie *et al.* 2019). The black dashed line indicates the Japan Trench axis. Axes  $X$  and  $Y$  are normal to and parallel to the trench axis, respectively. The white dashed lines are 100 km from axis  $X$  and  $Y$ . (b)  $V_p$  model obtained from a seismic survey along the line A6 (Fujie *et al.* 2019), corresponding to the range of the red solid line on (a). (c) Cross-section of the initial  $V_p$  model along axis  $X$ . Inverted triangles indicate projected location of the OBSs.

**Figure S2.** Initial model and results of the double-difference tomography analysis. (a) Map showing results of the tomography analysis for  $V_p$  at 20 km depth. Inverted triangles are the OBS locations. (b, c) Cross-sections of  $V_p$  (b) and  $V_s$  (c) along  $X-X'$  profile on axis  $X$  indicated by thick solid line on (a). Inverted triangles indicate OBS locations projected onto axis  $X$  (plotted at the top of the panel regardless of water depth). Dotted lines indicate  $V_p$  of 7 km s<sup>-1</sup> contour along A6 profile on panel Fig. S1(b) projected onto axis  $X$  and 7 km above it, which roughly correspond to the oceanic Moho and the top of the oceanic crust, respectively. (d) Map showing results of the checkerboard resolution test for  $V_p$  at 20 km depth. (e, f) Results of checkerboard resolution test for  $V_p$  (e) and  $V_s$  (f) along  $X-X'$  profile on axis  $X$  indicated by thick solid line on (d).

**Figure S3.** Hypocentre errors estimated from the bootstrap samples. (a) Maps showing error ellipsoids of hypocentre locations. Error ellipsoids are colour-coded by location error. Inverted triangles are OBS locations. The black dashed line indicates the Japan Trench axis. (b) Cross-section showing hypocentre errors projected onto the  $X-X'$  profile is indicated by the thick solid line in (a), which is the same as that in Fig. 3. Dotted lines roughly correspond to the top of the oceanic crust and oceanic Moho (as in Fig. S2b). Inverted triangles indicate OBS locations projected onto the profile (plotted at the top of the panel regardless of water depth).

**Figure S4.** Vertical component seismograms of the earthquakes located beneath the trench landward slope near the trench. (a) Map showing the locations of the OBSs (inverted triangles) and hypocentres (circles colour-coded by depth). Open circles indicate the tremors located by Ohta *et al.* (2019). Black circles (A–C) indicate the clusters of the shallow earthquakes. Arrows are horizontal displacement rates relative to the North American Plate (Honsho *et al.* 2019). (b, c, d) Vertical component seismograms of the earthquakes included in the cluster A, B and C are observed at JJB02A, JJB03A and JJB04A, respectively. The seismograms are normalized and aligned with the onset of the  $P$ -wave arrival.

Please note: Oxford University Press is not responsible for the content or functionality of any supporting materials supplied by the authors. Any queries (other than missing material) should be directed to the corresponding author for the paper.